Understanding the onset of negative electronic compressibility in single-band and two-band two-dimensional electron gases: Application to $LaAlO_3/SrTiO_3$

A. D. Mahabir,[1,2] A. V. Balatsky,[2,3] and J. T. Haraldsen[1]
[1]*Department of Physics, University of North Florida, Jacksonville, Florida 32224, USA*
[2]*Department of Physics, University of Connecticut, Storrs, Connecticut 06269, USA*
[3]*NORDITA, Roslagstullsbacken 23, 106 91 Stockholm, Sweden*

(Received 25 October 2020; revised 31 January 2021; accepted 1 March 2021; published 19 March 2021)

We investigate the effects of two electronic bands at the negative electronic compressibility (NEC) in a two-dimensional electron gas (2DEG). We use a simple homogeneous model with Coulombic interactions and first-order multiband coupling to examine the role of effective mass and relative permittivity in relation to the critical carrier density, where compressibility turns negative. We demonstrate that the population of a second band, along with the presence of interband coupling, can dramatically change the crossover carrier density. Given the difficulty in determining and confirming multiband electronic systems, this model provides a potential method for identifying multiband electronic systems using precise bulk electronic properties measurements. To help illustrate this method, we apply our results to the observed NEC in the 2DEG at the $LaAlO_3/SrTiO_3$ (LAO/STO) interface and determine that, for the known parameters of LAO/STO, the system is likely a realization of a two-band 2DEG. Furthermore, we provide general limits on the interband coupling with respect to the electronic band population.

DOI: 10.1103/PhysRevB.103.125141

I. INTRODUCTION

Complex oxide heterostructures have provided an exciting platform for various physical phenomena for over two decades, demonstrating the fascinating interplay between competing states depending on composition, doping, substitution, and structure [1,2]. Highly tunable electron-electron interactions at interfaces have been shown to host states with charge, spin, and orbital orderings [3–8] that emerge from the two-dimensional electron gas (2DEG) at the interface [9–14].

While there are many interesting properties of the 2DEG, we focus on the observations of negative electronic compressibility (NEC) [15,18,19]. NEC is produced through electron-electron interactions, where the exchange and Coulomb energies outweigh the overall kinetic energy of the electronic system [15–19]. Electronic compressibility is typically negative for dynamic, open two-dimensional (2D) systems [15,20–25] in nonequilibrium states, although recently, three-dimensional (3D) NEC systems have been discussed [26].

The 2DEG state of the complex oxide heterostructure $LaAlO_3/SrTiO_3$ (LAO/STO) exhibits a NEC. Over the last decade, measurements of the quantum capacitance have shown that the LAO/STO interface displays a large NEC around a carrier density of 10^{13} cm^{-2} [27–29]. Aside from NEC, LAO/STO interfaces were shown to host the possibly unconventional superconducting states at $T_c \sim 0.2$ K [30–32], which has led to fundamental questions about the nature of the superconducting state and its relation to the nature of the normal state [33–38]. It is also known that superconductivity can be enhanced to 0.3–0.4 K by applying an electric field [33,34] and is observed to increase with strain [39,40]. Therefore, there is an exciting possibility that NEC and superconductivity might be related.

Observations point to the very robust superconducting interactions in STO that are controlled by doping and dimensionality. Literature has shown that the electron mobility observed at the interface is related to the electronic states within STO alone and is not dependent on the adjacent material [29,35,37,38,41–45]. Furthermore, while still controversial, recent experiments have also found strong evidence that the maximum T_c in the heterostructures is achieved once an extra electron band becomes occupied [46]. Currently, there are a few proposals that the superconductivity in LAO/STO may be a realization of a multiband system [29,35,43–46], where band-structure calculations have illustrated the role of split bands in electronic transport as a function of doping [47]. However, this is not without controversy, as some reports indicate that this not the case [32,37,38,48], while for others the claim of multiband electronic structure still needs to be looked at carefully [3–5].

The determination of a multiband superconducting state is quite complicated as the multiband phenomenon's conclusive evidence can take decades due the difficulty in resolving the small energy gap between bands which is not well resolved by most techniques. However, not long after the theoretical basis [49], multiband superconductivity was discovered in transition-metal superconductors, including Nb-doped STO [42,50,51]. In the case of Pb superconductors, the theory suggested that two-band superconductivity was possible in 1965 [52], but it was not experimentally confirmed until 2000

[53], despite earlier experimental evidence [54]. Detailed *ab initio* calculations supporting the multiband scenario were performed in 2009 [55].

This paper aims to examine the differences in electronic compressibility between one- and two-band models and hopes to provide clarity and guidance for understanding the nature of collective electronic states at 2D interfaces (i.e., multiband superconductivity). Therefore, in this study, we examine the one- and two-band models of a 2DEG and investigate the onset of negative compressibility. Using a homogeneous 2D electron model and a two-band description of the electron interactions, we examine the dependence of the negative compressibility crossover point with respect to the carrier density. In general, we find the increase in effective mass leads to the rise in critical carrier density for NEC. In contrast, an increase in the relative permittivity of the 2DEG leads to a decrease in the critical carrier density. Furthermore, the addition of a second band lowers the overall crossover carrier density, where the presence of interband coupling will dramatically reduce the polarizability of the 2DEG. The analysis presented in this work establishes features in the bulk electronic properties that allow for the possible identification of multiple bands in 2DEG systems. Additionally, through the comparison with previous experimental results for LAO/STO [27–29,45], we find that the NEC of LAO/STO is consistent with a two-band model of the 2DEG, which provides further evidence that the LAO/STO interface electron states may be a realization of a multiband system. Our findings also provide a straightforward method for the identification of electron band populations and coupling between the bands.

The structure of the paper is as follows: After the Introduction, we discuss the general attributes of the negative compressibility state in Sec. II. In Sec. III, we revisit the electron gas free energy calculation for the multiband case. In Sec. IV, we discuss our results in the context of the LAO/STO interface and we conclude in Sec. V with a summary of the results.

II. ELECTRONIC COMPRESSIBILITY

Electronic compressibility, the response of the chemical potential to changes in the carrier density, is given by

$$\kappa = \left(n^2 \frac{d\mu}{dn}\right)^{-1}, \tag{1}$$

where μ is the chemical potential and n is the carrier density. Typically, an increase in the carrier density produces a positive increase of the chemical potential [20,28]. Because of standard thermodynamic constraints, electronic compressibility tends to be positive. However, if the system is interacting, in some cases, the compressibility shift is negative, resulting in the so-called negative electronic compressibility [56]. NEC is typically found in 2D materials due to topological effects [15,20,21,23,24]. Recently it has also been suggested in 3D materials [26].

If we assume a two-band model with simple parabolic dispersion (as shown in Fig. 1), then as the chemical potential increases to $\mu/\mu_c = 1$, the second band becomes populated and the carrier density will increase. At a critical density, one will see a dramatic increase in the density of states (DOS)

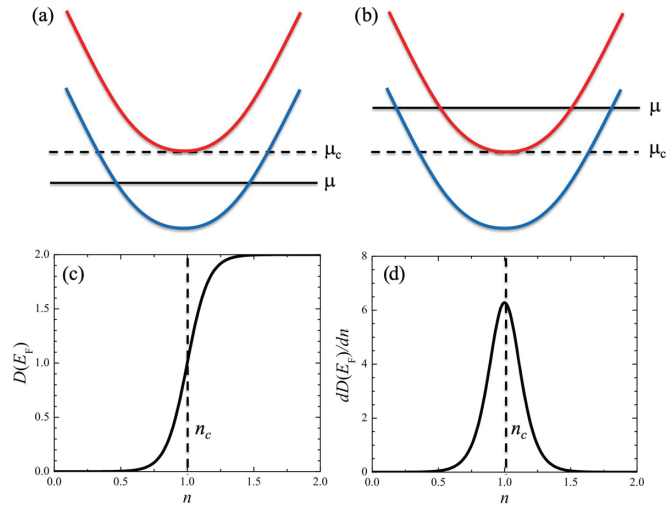

FIG. 1. Illustration of the two-band model with (a) $\mu < \mu_c$ and (b) $\mu > \mu_c$. (c) The DOS as a function of n for the two-band system. (d) $dD(E_F)/dn$ as function of n.

$D(E_F)$ [shown in Fig. 1(c)] as a result of the second band being populated.

We start with inverse compressibility κ^{-1} being proportional to $d\mu/dn$, which can be written as

$$\frac{d\mu}{dn} = \frac{d\mu}{dD(E_F)} \frac{dD(E_F)}{dn}, \tag{2}$$

where $dD(E_f)/dn$ is essentially $\delta(D(E_F) - n)$. Given a standard experimental width, $dD(E_F)/dn$ will resemble Fig. 1(d).

For a 2DEG at $T = 0$, the chemical potential is equivalent to the Fermi energy E_F [15]. Using a standard parabolic dispersion,

$$\mu = E_F = \frac{\hbar^2 k_F^2}{2m^*}, \tag{3}$$

where k_f is the Fermi wave vector and m^* is the effective mass given in units of the electron mass, m_e. For a 2D system, the number of states per unit area is $N = \frac{k_F^2}{2\pi}$. Thus the DOS is well known as

$$D(E_F) = \frac{dN}{dE_F} = \frac{m^*}{\pi\hbar^2}. \tag{4}$$

From this relationship, we can infer that

$$\frac{d\mu}{dD(E_F)} = \frac{dk_F^2/2m^*}{dm^*} = -\frac{\pi\hbar^4 k_F^2}{2m^{*2}}. \tag{5}$$

This result provides an important clue about the origin of a negative contribution to the compressibility: the negative sign appears as chemical potential *decreases* with the effective mass per same carrier density. Therefore, to gain an understanding of when the electronic compressibility for a two-band system becomes negative, we need to understand the free energy of electron gas in the system.

The chemical potential is defined as the change in free energy over the change in the number of electrons, N_e,

$$\mu = \frac{dF}{dN} = \frac{df}{dn}, \tag{6}$$

where $f = F/A$ is the free energy divided by the area. One can relate the chemical potential to the density by normalizing the system by the area A, which allows us to define the electronic compressibility in terms of the free energy and the carrier density since $d\mu/dn = d^2f/dn^2$:

$$\kappa = \left(n^2 \frac{d^2 f}{dn^2}\right)^{-1}. \tag{7}$$

Since most experimental measurements examine the $d\mu/dn$, we will use inverse compressibility κ^{-1} to discuss the crossover between positive and negative compressibility.

It is important to note that, in many systems, the effective mass and Fermi wave vector are direction dependent. Here, we assume a simplified isotropic model.

III. 2D ELECTRON GAS FREE ENERGY

Focusing on carrier density dependence of the free energy [15], we decompose f into kinetic [16,17], exchange [22,57], and Coulomb components [58,59] ($f = f_k + f_{ex} + f_c$) using an analytic model [60], and examine each component individually for each band. Based on a homogeneous 2D electron model,

$$f_k = \sum_i \frac{\pi n_i^2 \hbar^2}{2m_i^*},$$

$$f_{ex} = -\sum_i \sqrt{\frac{2n_i^3}{\pi}} \frac{e^2}{3\pi\epsilon_{\text{eff}}},$$

$$f_c = \sum_i n_i^2 \frac{\alpha a_B e^2}{2\epsilon_{\text{eff}}} - \sum_i \sqrt{\frac{n_i^3}{\pi}} \frac{e^2}{2\epsilon_{\text{eff}}}, \tag{8}$$

where the Coulomb or electrostatic term is broken into in-plane and out-of-plane components. Here, $\epsilon_{\text{eff}} = \epsilon_r \epsilon_0$ (the effective dielectric constant), and e is the electron charge, αa_B is the effective distance between layers, a_B is the Bohr radius $4\pi\epsilon_0\hbar^2/m^*e^2$, and α is a phenomenological tuning parameter for the out-of-plane electrostatic part of free energy. The out-of-plane electrostatic confinement term is needed for 2DEG materials with strong polarization. Overall, the full free energy is summed over i bands, where $i = 2$ is the specific case we consider. This free energy is a general analytic model and is meant to examine the general nature of the 2DEG in the absence of more complicated interactions. Therefore, we are using this model to detail qualitative features understand the differences between one- and two-band systems.

A. One-band model

Using the free energy for a one-band 2DEG, the inverse electronic compressibility can be shown to be

$$\kappa^{-1} = n^2 \left(\frac{\pi\hbar^2}{m^*} + \frac{4\alpha\pi\hbar^2}{m^*\epsilon_r} - \frac{3e^2}{8\sqrt{n\pi}\epsilon_{\text{eff}}} - \sqrt{\frac{2}{n\pi^3}} \frac{e^2}{4\epsilon_{\text{eff}}} \right), \tag{9}$$

where the effects of the parameters are shown in Fig. 2. Here, we present the inverse electronic compressibility as a function of the carrier density for various effective electron masses and

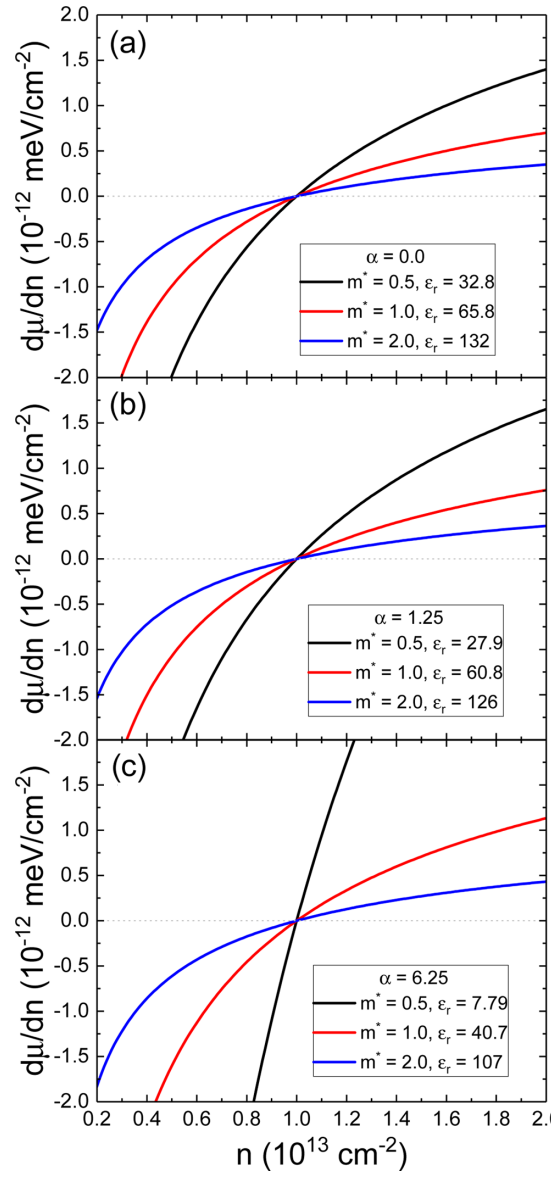

FIG. 2. The inverse electronic compressibility for the one-band model plotted as a function of carrier density for various effective masses and out-of-plane electrostatic parameters (a) $\alpha = 0$, (b) $\alpha = 1.25$, and (c) $\alpha = 6.25$. The quoted relative permittivities are given as the permittivity needed for the crossover carrier density to be $n_c = 1 \times 10^{13}$ cm^{-2}. All effective masses are in units of the electron mass.

relative permittivities as well as with and without the presence of out-of-plane electrostatic confinement. Here, we have chosen parameters for the effective mass and relative permittivity that will provide a crossover carrier density of 1.0×10^{13} cm^{-2} for various values of out-of-plane electrostatic parameter α. The crossover points indicate carrier densities where electronic compressibility switches from positive and negative. These densities correspond to a regime where a second band is populated. When compared to experimental results, it is not just the value of the crossover carrier density but also the line's overall slope through the point that matters. The slope of the electronic compressibility through the critical point appears to be greatest when effective masses and permittivities

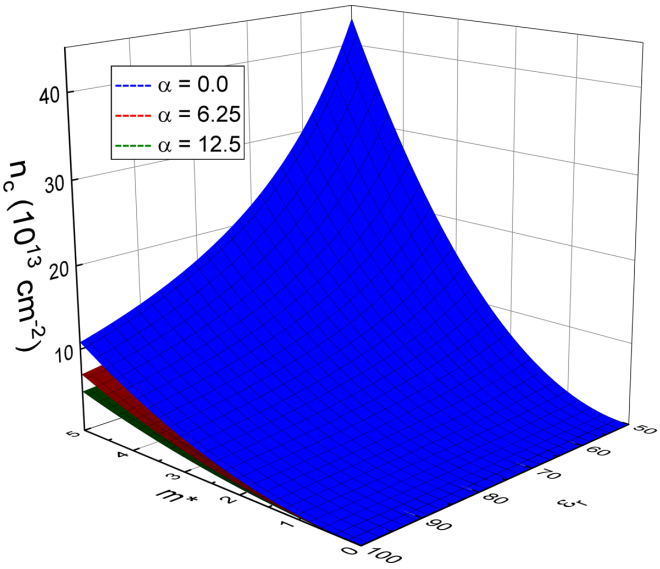

FIG. 3. Crossover carrier density for the one-band model as a function of effective mass and relative permittivity for $\alpha = 0$ (blue, top), 6.25 (red, middle), and 12.5 (green, bottom). All effective masses are in units of the electron mass.

are lowest, which indicates a greater increase in chemical potential with carrier density.

Since the inverse electronic compressibility is proportional to the change in the chemical potential with regards to n, we can determine the critical crossover carrier density n_c for the one-band model by solving $d\mu/dn = 0$, and show that

$$n_c = \frac{(3\pi + 2\sqrt{2})^2}{64\pi^3(\epsilon_r + 4\alpha)^2}\left(\frac{m^* e^2}{\pi\epsilon_0\hbar^2}\right)^2. \tag{10}$$

Here, the crossover carrier concentrations depend on the square of the effective mass over relative permittivity for the 2DEG. The addition of an out-of-plane electrostatic confinement field lowers the carrier density for negative electronic compressibility (shown in Fig. 3), where it is demonstrated that the crossover carrier density is controlled by effective mass, relative permittivity, and z-axis electrostatic potential. Within the general understanding of electrodynamics, an increasing effective mass will increase the number of states at the Fermi level, lower the overall kinetic energy of the electronic system, and increase the critical carrier density for the transition.

Figure 3 shows that an increase in the relative permittivity leads to the decrease in the critical carrier density. The plots for larger values of α follow the same trend as the $\alpha = 0$ curve with an overall lowering of the critical carrier density. We interpret this effect being due to a decrease in the exchange and Coulomb interactions. This effect is also accompanied by increase of the out-of-plane electrostatic confinement.

These changes in the permittivity with carrier density are consistent with the general understanding of electronic structure. The lower the carrier density, the more insulating the material becomes, resulting in enhanced polarizability for the material. It is also shown that increasing the effective mass will also increase the needed permittivity due to the reduction in the conductivity, which will localize charge and allow for higher polarizabilities.

B. Two-band model

Since the crossover carrier density of 2DEG is a measure of band population, there should be distinct differences in the effects of a one-band system regarding a two-band system. Therefore, we generalize the previous analysis to a two-band case and slightly alter the model by adding the first-order coupling between bands.

Assuming a two-band model ($i = 1, 2$), we have

$$\begin{aligned} f = &\left(\frac{\pi\hbar^2}{2} + \frac{2\pi\alpha\hbar^2}{\epsilon_r}\right)\left(\frac{n_1^2}{m_1^*} + \frac{n_2^2}{m_2^*}\right) \\ &- \sqrt{\frac{2}{\pi^3}}\frac{e^2}{\epsilon_{\text{eff}}}\left(\frac{1}{3} + \frac{\pi}{\sqrt{2^3}}\right)\left(n_1^{\frac{3}{2}} + n_2^{\frac{3}{2}}\right) \\ &+ \frac{\lambda\pi\hbar^2}{2\sqrt{m_1^* m_2^*}} n_1 n_2, \end{aligned} \tag{11}$$

where λ provides a first-order coupling between the two bands within a Ginzburg-Landau approximation, where this term is considered isotropic to help reduce the overall number of parameters. Since the interaction can be either repulsive or attractive, λ can be either positive or negative. Here, the total interaction energy between two bands can be expanded as an ordered series of terms. We are considering only the first-order term, which is linear in both n_1 and n_2. Higher-order terms and other interactions could also be included, but they are typically system specific and move us away from this more general model.

From the free energy model, the inverse electronic compressibility κ^{-1} can now be written as

$$\begin{aligned} \kappa^{-1} = n^2\Bigg[&\left(\pi\hbar^2 + \frac{4\pi\alpha\hbar^2}{\epsilon_r}\right)\left(\frac{\eta^2}{m_1^*} + \frac{(1-\eta)^2}{m_2^*}\right) \\ &- \frac{e^2}{4\epsilon_{\text{eff}}\sqrt{n}}\left(\sqrt{\frac{2}{\pi^3}} + \frac{3}{2\sqrt{\pi}}\right)\left(\eta^{\frac{3}{2}} + (1-\eta)^{\frac{3}{2}}\right) \\ &+ \frac{\lambda\pi\hbar^2(\eta - \eta^2)}{\sqrt{m_1^* m_2^*}}\Bigg]. \end{aligned} \tag{12}$$

Here, we define the total carrier density $n = n_1 + n_2$ and relative population factor η, where $n_1 = \eta n$ and $n_2 = (1-\eta)n$. Therefore, η provides a simple gauge that changes the electron population from one band to the other and is assumed to be independent on the carrier density. In the case of $\eta = 1$ or 0 the carrier population is solely in the first or second band. Any fractional concentration ratio describes carriers shared between bands; $\eta = 0.5$ corresponds to both bands being equally populated.

As shown for the one-band model, Fig. 4 shows the inverse electronic compressibility as a function of the 2D carrier density for the two-band system with various coupling interactions λ, density ratios η, and effective masses. To illustrate the effect of α, the data with critical crossover points at 1.0×10^{13} cm^{-2} have a value of $\alpha = 0$, while those at 0.5×10^{13} cm^{-2} have a value of $\alpha = 12.5$.

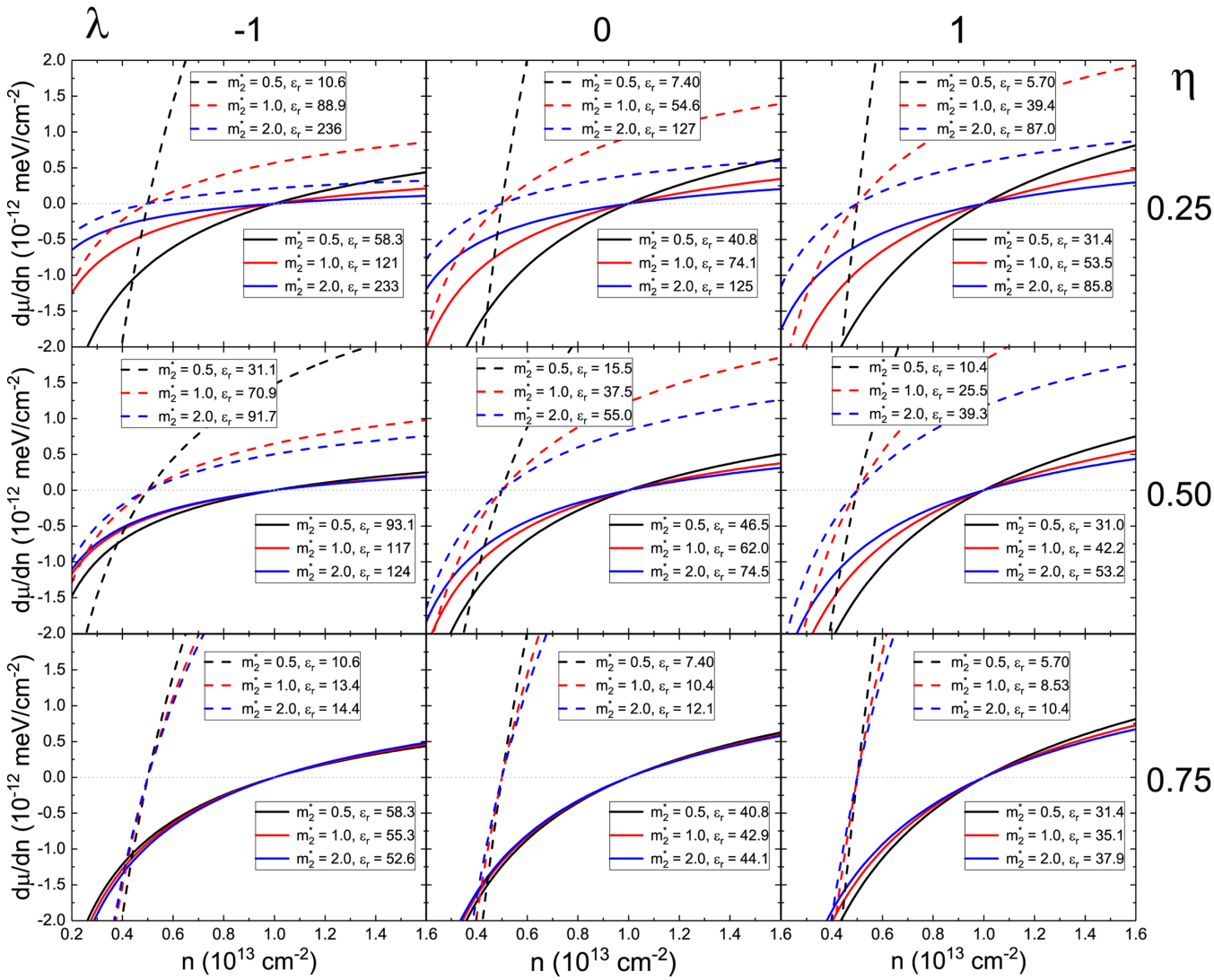

FIG. 4. The inverse electronic compressibility as a function of carrier density for the two-band system with various coupling interactions $\lambda = -1$, 0, and 1 and density ratios $\eta = 0.25$, 0.50, and 0.75. Within each plot, the inverse electronic compressibility is plotted for different effective masses. The out-of-plane electrostatic factor and the relative permittivity have been selected to make $n_c = 1.0 \times 10^{13}$ cm^{-2} ($\alpha = 0.0$) or 0.5×10^{13} cm^{-2} ($\alpha = 12.5$). All effective masses are in units of the electron mass.

Similar to the one-band model, the lower effective masses produce a sharper slope of the curve through the critical points. The addition of a second band enhances the slope further as λ or α is increased, where the dramatic increase in slope requires a lower effective dielectric constant. A general effect of the two-band model is the need for lower overall polarizability to achieve the same crossover carrier density, which leads to the suggestion that the combination of effective mass and dielectric measurements can help distinguish between one- and two-band systems.

To examine these effects further, we focus on the crossover carrier density for the inverse electronic compressibility, given by

$$n_c = \frac{(3\pi + 2\sqrt{2})^2}{64\pi^3(\epsilon_r + 4\alpha)^2}\left(\frac{\sqrt{m_1^* m_2^*}e^2}{\pi\epsilon_0\hbar^2}\right)^2 \times \left(\frac{\eta^{3/2} + (1-\eta)^{3/2}}{1/\gamma\eta^2 + \sqrt{\gamma}(1-\eta^2) + \lambda\eta(1-\eta)}\right)^2, \quad (13)$$

where $\gamma = m_1^*/m_2^*$. Here, it is clear that the first part of the equation is the one-band model, and the second part details the second-band adjustment. In a similar manner as the one-band model, Fig. 5 shows the critical carrier density as a function of relative permittivity and effective mass of the second band with different values of λ and η. Here, the first band's effective mass is set to 0.5 and $\alpha = 0$. Similar trends in the one-band system also can be observed. Larger critical carrier density occurs in systems with larger effective masses and lowers relative permittivities. Figure 5 illustrates the effect of λ and η on the critical carrier density as a function of ϵ_r and m_2^*.

In Fig. 6, the effects of η and λ on the crossover carrier density with $m_2^* = 0.5m_e$ and $1.0m_e$ and $\alpha = 0.0$ and 12.5 are detailed. Here, m_1^* is held at $0.5m_e$ and $\epsilon_r = 50$, and shows that the sharing of carrier density between the bands increases the critical carrier density. This effect is illustrated best when the effective masses are equal. Here, the critical carrier density is symmetric about $\eta = 0.5$, and η results in shifting of electrons towards the one-band regime and produces higher carrier

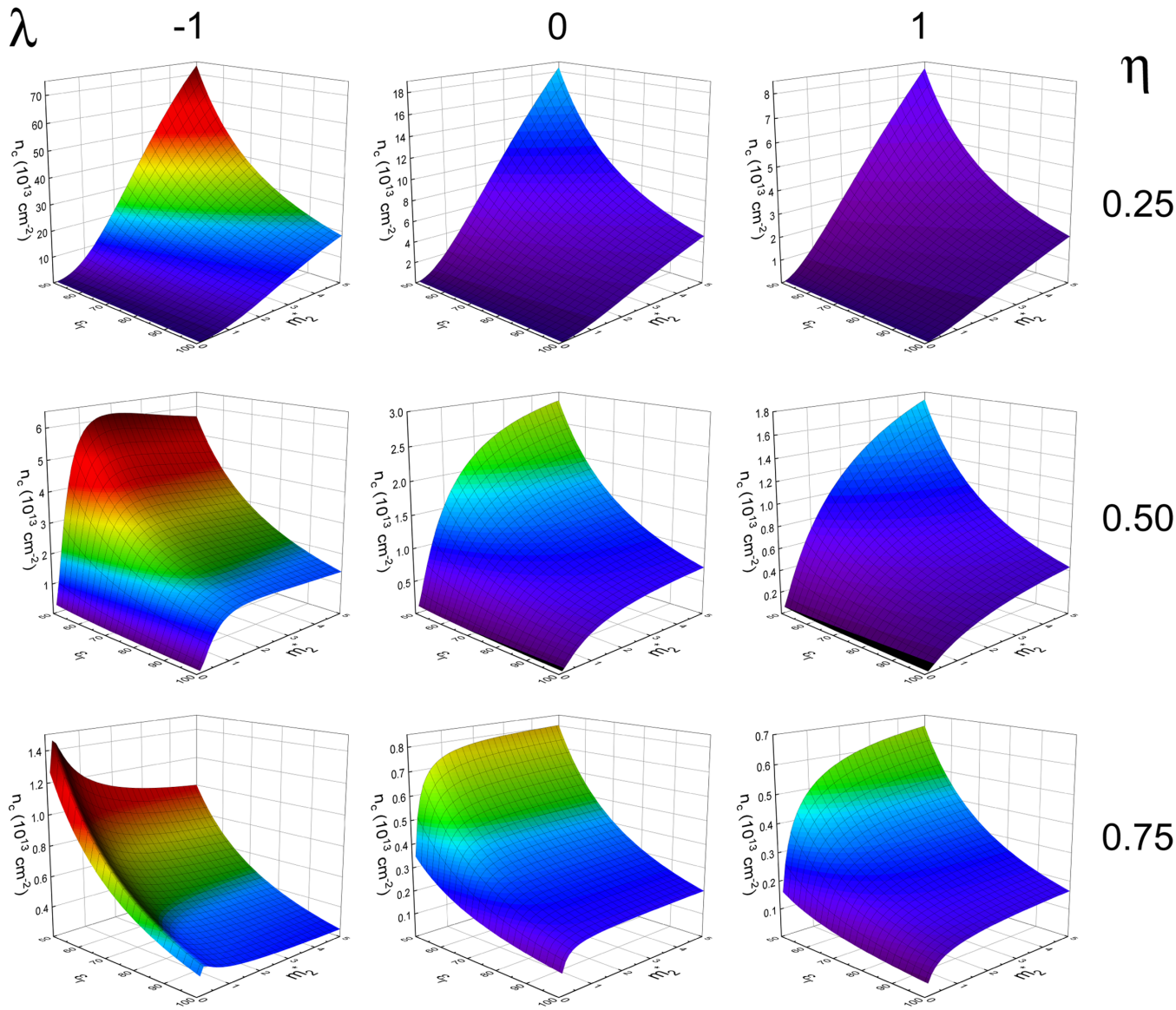

FIG. 5. The critical carrier density as a function of ϵ_r and m_2^* for different values of λ and η with $m_1^* = 0.5m_e$ and $\alpha = 0$. The color scales for each row of plots are set by the $\lambda = -1$ column to detail the shift in carrier density. All effective masses are in units of the electron mass.

density regions with increasing effective mass. It is important to note that the critical carrier density continues to increase beyond the $\lambda = -1$ plane. Therefore, with respect to a given λ, the critical carrier density will peak at a given η, but for a given η, there is no global maximum.

From Eq. (13), we see some overall trends: (i) as the density ratio is shifted from the equal point of $\eta = 0.5$, the electronic system requires an overall increase permittivity and becomes more apparent with a negative λ; (ii) as λ increases in value, the needed relative permittivity is decreased. While the overall dependence of the critical carrier density from the effective permittivity and masses is similar to the one-band model, examining the combination of measured parameters can help determine the likelihood of either a one- or two-band system.

By looking at the $\eta = 0.5$ and $\lambda = 0$ case in Fig. 4, the critical carrier density response is quite similar to that of the one-band model. If one includes band interactions the crossover points shift depending on the type of interaction and strength: for increasing λ, the critical point shifts as the required permittivity decreases.

To further examine the effects of multiband interactions, we focus on the example of the LAO/STO interface, where some experiments have indicated that the system is possibly in the multiband regime [42,46,61].

IV. RELEVANCE TO LAO/STO INTERFACES

The interface of $LaAlO_3$ (LAO) and $SrTiO_3$ (STO) has become a textbook example of the emergence of complex phenomena at complex oxide interfaces where two-band insulators produce a 2DEG, which becomes superconducting at 200–300 mK [30–32]. Studies into the nature of the superconducting state at the LAO/STO interface have revealed the potential for a multiband electronic system [29,35,43,44,47]. On the other hand, there is a significant body of literature

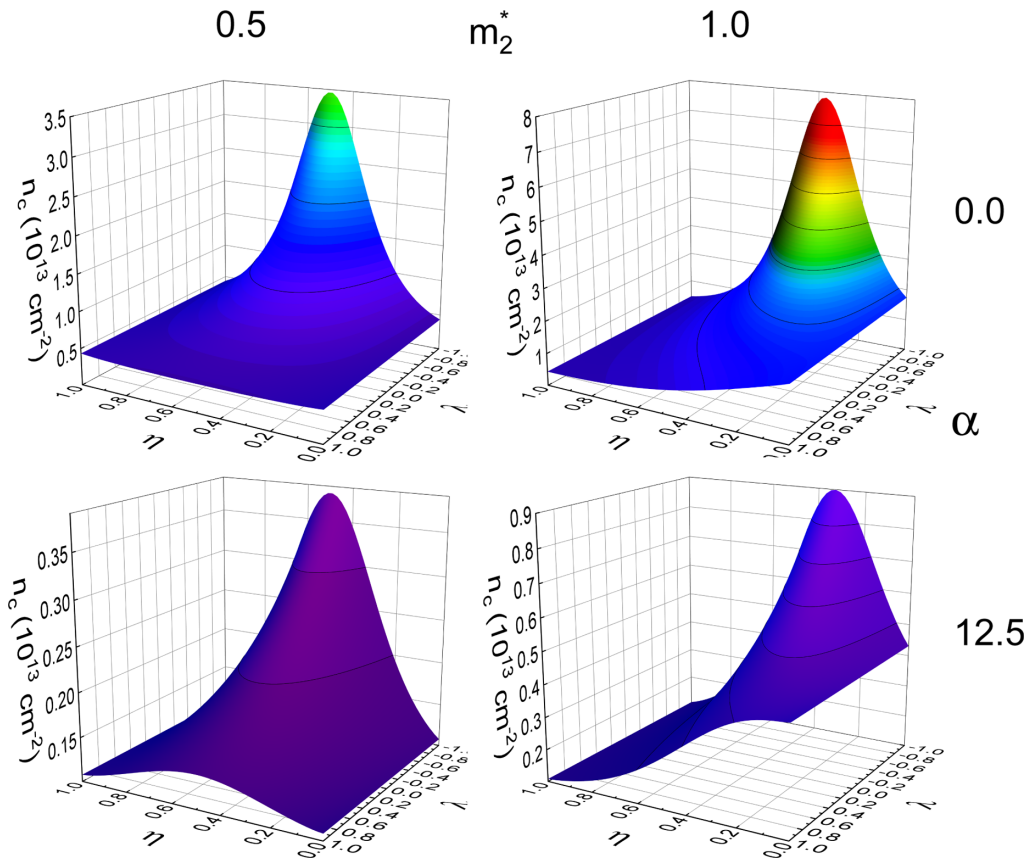

FIG. 6. The effects of η and λ on the crossover carrier density with $m_2^* = 0.5m_e$ and $1.0m_e$ and $\alpha = 0.0$ and 12.5. Here, m_1^* is held at $0.5m_e$ and $\epsilon_r = 50$.

that seems to indicate that the interfacial electronic states correspond to a single band [62–65]. Therefore, to provide a method that could help identify multiband electronic systems, we present an approach based on observable properties of the normal electronic states. However, the difference occurs in the material parameters' values, which is one reason multiband systems are challenging to identify. It is not in the curvature or functional form of the potential, but a precise analysis of measured parameters.

Electron-doped n-type STO exhibits a distinct transition into a superconductor with a peak $T_c = 200$ mK. Moreover, theoretical and experimental studies have shown that the superconducting transition can be dramatically enhanced under pressure [39,40]. In Ref. [35] we described multiband aspects of this superconductivity and discussed the similarities between bulk STO and the LAO/STO interface. In the present work we adopt this two-band model for the general case of normal state 2DEGs to the LAO/STO interface to determine the most relevant features.

To make a relevant comparison we would need to determine values of dielectric constant for interfaces. For the bulk systems, LAO has a measured dielectric constant of about 18–24 [66,67]. In contrast, STO can have a dielectric constant upwards of 25 000 at zero electric field, and drops to around 300 (with an electric field or at high temperatures) [66,68]. Since the 2DEG exists in the STO layer with a typical depth of 5–7 nm [69], the results of the analysis of the two-band model depend greatly on the measured value of the dielectric constant and the effective mass. To be specific, we assume a range of dielectric constants between about 70 and 150 [6,7,45,70–76], and estimated effective masses for the LAO/STO range from $0.5m_e$ to $0.7m_e$ for the first band and $5.0m_e$ to $14m_e$ for the second band [70].

In LAO/STO, the critical carrier density is very device dependent and seems to fall between 0.5 and 1.0×10^{13} cm^{-2} [27]. With these ranges in mind, Fig. 7 shows the carrier density as a function of relative permittivity and effective mass for two different electrostatic parameters for the one-band model. The parameter ranges for LAO/STO have been shaded in grey. Through the middle, the brown contour shows the permittivity and effective mass range for the general critical carrier density range of LAO/STO. In Fig. 7(a), the measured LAO/STO parameters come very close to falling into the carrier density range for $\alpha = 0$. However, suppose one includes an out-of-plane electrostatic energy [Fig. 7(b)], which is needed for the polar heterostructure of LAO/STO. In that case, the parameters become even further apart. Therefore, given the wide range of device-specific measurements, it seems that the one-band model is not applicable.

Figure 8 shows the carrier density as a function of relative permittivity and effective mass for two different electrostatic parameters for the two-band model. The main issue is that we do not know the relative population of the bands or the coupling constant. Therefore, by using the closest parameters from the one-band model ($\epsilon_r = 70$ and $m_1^* = 0.7m_e$) and instituting a second-band effective mass of $14m_e$, we show the

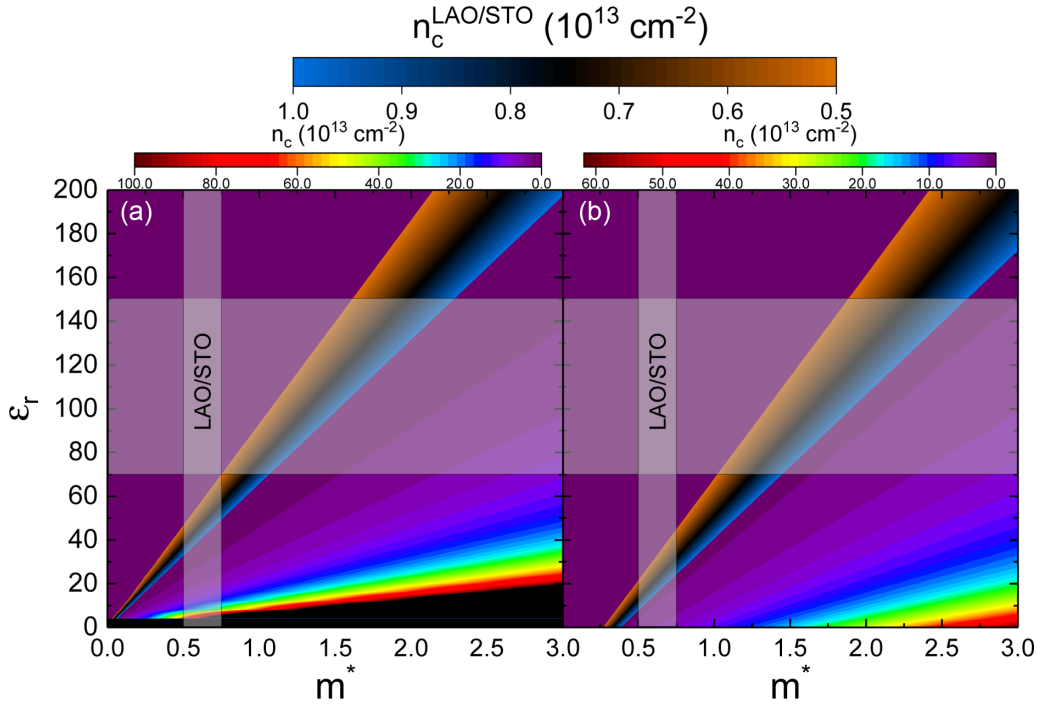

FIG. 7. The critical crossover carrier density is plotted as a function of relative permittivity and effective mass for the one-band model with (a) $\alpha = 0$ and (b) $\alpha = 12.5$. The shaded region illustrates the regime where most measurements of the relative permittivity and effective mass of LAO/STO are performed. Within our model, we conclude that the behavior the known LAO/STO parameters do not fall within the predicted behavior of a one-band model. All effective masses are in units of the electron mass.

range of η and λ needed to provide critical carrier density of between 0.5 and 1.0×10^{13} cm^{-2} for $\alpha = 0.0$ and 12.5 (without and with electrostatic confinement).

We conclude that the band filling never falls on $\eta = 1$ or 0; hence we assume that a two-band model is needed to account for the measured electronic parameters of LAO/STO. Furthermore, if the system demonstrates larger effective mass or a lower permittivity, then the LAO/STO interface may reduce back to a one-band model (as shown in Fig. 7), which is why we have chosen parameters that appear to be on the limits of measured quantities for this system. Therefore, our model provides a useful tool for experimentalists to investigate the multiband model.

Our approach demonstrates that effective masses for the 2DEG must be reasonably small for the first band to produce a similar compressibility slope and dielectric constant. We find more flexibility with the interband coupling and variable carrier density within a two-band model.

Overall, the proposed two-band 2DEG model demonstrates that stronger interband coupling lowers the required ϵ_r for the system. The coupling of the bands produces less electron screening. It makes the system less metallic, consistent with Fernandes *et al.* [35], where it was shown that a weakly interacting two-band model adequately describes the 2D STO system. Our analysis indicates that, within the 2DEG model, a two-band or multiband system is adequately describing the LAO/STO interface [35,42]. We also mention multiple experimental observations suggesting the multiband nature of 2DEGs [29,43–45].

It should be mentioned that this analysis is done with an isotropic model. However, in the LAO/STO system, the second band being occupied is a doubly degenerate band with a fairly anisotropic effective mass that can range from $5m_e$ to $14m_e$ depending on the orientation [46,48]. Therefore, in our analysis, we have chosen to use a large effective mass of $14m_e$ for the second band, which illustrates that the system still prefers the multiband model over the single band.

V. CONCLUSIONS

In this paper, we provide a general method for determining the effects of multiband interactions on a two-dimensional electron gas through electronic compressibility. Using a 2D electron gas model with a first-order interband coupling between the carrier densities, we examine the dependence of negative compressibility of the 2D electron gas on critical carrier density, dielectric constant, and effective mass and compare the results to the $LaAlO_3/SrTiO_3$ interface. Our calculations show that the presence of interband coupling has an effect on the polarizability and the critical carrier density of the 2DEG. Furthermore, we find that the bands' effective masses have a distinct and dramatic effect on the negative compressibility.

Given recent suggestions that the LAO/STO interface is a multiband electron system [29,35,43,44], we relate the negative compressibility to interband and intraband interactions and to the effective electron masses in the bands. We find that a one-band model does not reproduce the LAO/STO

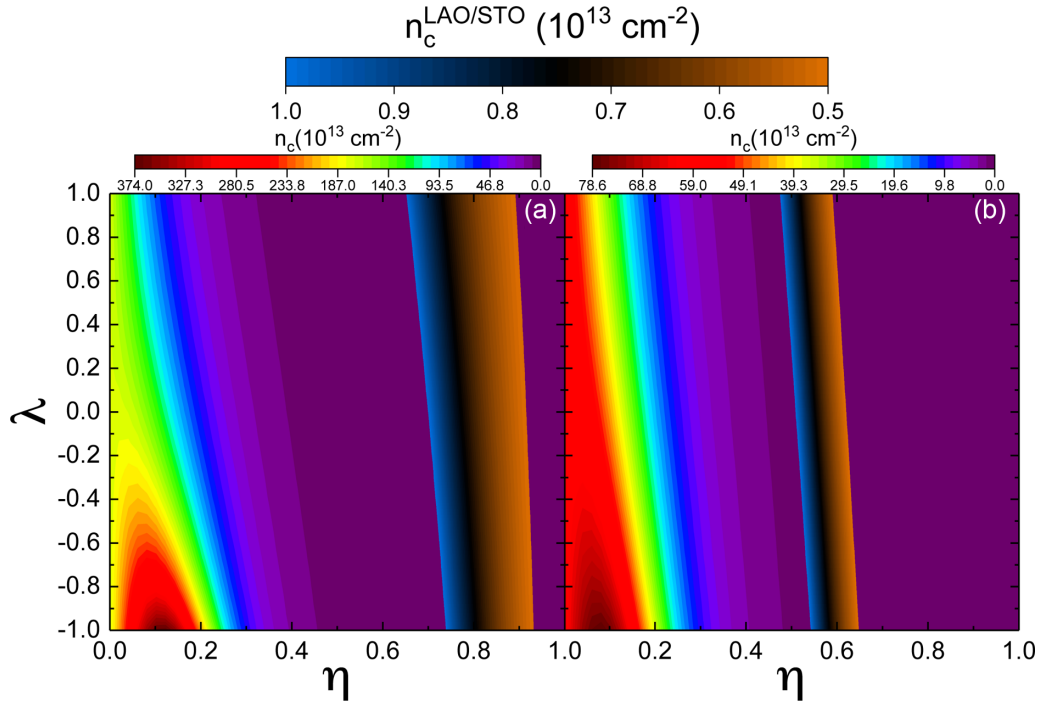

FIG. 8. The critical crossover carrier density is plotted as a function of λ and η for the closest LAO/STO parameters ($\epsilon_r = 70$, $m_1^* = 0.7m_e$, and $m_2^* = 14m_e$) for the two-band model with (a) $\alpha = 0$ and (b) $\alpha = 12.5$. The blue/brown cone region denotes the LAO/STO critical carrier density region and provides a multiband parameter space for experimentalists to investigate the presence of the two-band electronic states in these devices.

interface's critical carrier density. On the other hand, using a two-band model, we find the critical carrier density for the negative compressibility crossover of LAO/STO within the parameter range that is consistent with the observations.

Among future applications of the model presented here, we mention the effects of dynamics on electronic properties like transport and compressibility. For example, the role of dynamics and pumping in producing the transient negative compressibility regime in multiband 2DEG would be an interesting problem to pursue. We also point to the important questions about the nature of the superconducting state, seen in LAO/STO, in the presence of two coupled electronic bands.

ACKNOWLEDGMENTS

The authors would like to thank the referees, especially the second referee, for their insight and helpful comments. Additionally, A.D.M. and J.T.H. would like to acknowledge support by the Institute for Materials Science at Los Alamos National Laboratory. The work of A.V.B. was supported by the University of Connecticut, VILLUM FONDEN via the Centre of Excellence for Dirac Materials (Grant No. 11744), the European Research Council under the European Union's Seventh Framework Program Synergy HERO, and KAW.

[1] J. Heber, Materials science: Enter the oxides, Nature **459**, 28 (2009).

[2] W. Prellier, M. Singh, and P. Murugavel, The single-phase multiferroic oxides: From bulk to thin film, J. Phys.: Condens. Matter **17**, R803 (2005).

[3] D. Khomskii and G. Sawatzky, Interplay between spin, charge and orbital degrees of freedom in magnetic oxides, Solid State Commun. **102**, 87 (1997).

[4] P. Zubko, S. Gariglio, M. Gabay, P. Ghosez, and J.-M. Triscone, Interface physics in complex oxide heterostructures, Annu. Rev. Condens. Matter Phys. **2**, 141 (2011).

[5] J. Chakhalian, J. Freeland, H. Habermeier, G. Cristiani, G. Khaliullin, M. van Veenendaal, and B. Keimer, Orbital reconstruction and covalent bonding at an oxide interface, Science **318**, 1114 (2007).

[6] H. Lee, N. Campbell, J. Lee, T. Asel, T. Paudel, H. Zhou, J. Lee, B. Noesges, J. Seo, B. Park, L. Brillson, S. Oh, E. Tsymbal, M. Rzchowski, and C.-B. Eom, Direct observation of a two-dimensional hole gas at oxide interfaces, Nat. Mater. **17**, 231 (2018).

[7] M. Reinle-Schmitt, C. Cancellieri, D. Li, D. Fontaine, M. Medarde, E. Pomjakushina, C. Schneider, S. Gariglio, P. Ghosez, J.-M. Triscone, and P. Willmott, Tunable conductivity threshold at polar oxide interfaces, Nat. Commun. **3**, 932 (2012).

[8] J. T. Haraldsen, P. Wölfle, and A. V. Balatsky, Understanding the electric-field enhancement of the superconducting transition temperature for complex oxide interfaces, Phys. Rev. B **85**, 134501 (2012).

[9] Y. Kozuka, A. Tsukazaki, D. Maryenko, J. Falson, S. Akasaka, K. Nakahara, S. Nakamura, S. Awaji, K. Ueno, and M. Kawasaki, Insulating phase of a two-dimensional electron gas in $Mg_xZn_{1-x}O$/ZnO heterostructures below $\nu = \frac{1}{3}$, Phys. Rev. B **84**, 033304 (2011).

[10] J. W. Park, D. Bogorin, C. Cen, D. Felker, Y. Zhang, C. Nelson, C. W. Bark, C. Folkman, X. Pan, M. Rzchowski, J. Levy, and C.-B. Eom, Creation of a two-dimensional electron gas at an oxide interface on silicon, Nat. Commun. **1**, 94 (2010).

[11] V. N. Popok, P. A. Caban, P. P. Michalowski, R. Thorpe, L. C. Feldman, and K. Pedersen, Two-dimensional electron gas at the AlGaN/GaN interface: Layer thickness dependence, J. Appl. Phys. **127**, 115703 (2020).

[12] E. V. Kirichenko, V. A. Stephanovich, and V. K. Dugaev, Conductivity of the two-dimensional electron gas at $LaAlO_3/SrTiO_3$ interface, Phys. Rev. B **95**, 085305 (2017).

[13] D. Pesquera, M. Scigaj, P. Gargiani, A. Barla, J. Herrero-Martín, E. Pellegrin, S. M. Valvidares, J. Gázquez, M. Varela, N. Dix, J. Fontcuberta, F. Sánchez, and G. Herranz, Two-Dimensional Electron Gases at $LaAlO_3/SrTiO_3$ Interfaces: Orbital Symmetry and Hierarchy Engineered by Crystal Orientation, Phys. Rev. Lett. **113**, 156802 (2014).

[14] S. Stemmer and S. James Allen, Two-dimensional electron gases at complex oxide interfaces, Annu. Rev. Mater. Res. **44**, 151 (2014).

[15] M. Bello, E. Levin, B. Shklovskii, and A. Efros, Density of localized states in the surface impurity band of a metal-insulator-semiconductor structure, Zh. Eksp. Teor. Fiz. **80**, 1596 (1981) [Sov. Phys. JETP **53**, 822 (1981)].

[16] T. Kopp and J. Mannhart, Calculation of the capacitances of conductors—perspectives for the optimization of electronic devices, J. Appl. Phys. **106**, 064504 (2009).

[17] B. Tanatar and D. Ceperley, Ground state of the two-dimensional electron gas, Phys. Rev. B **39**, 5005 (1989).

[18] A. M. J. Schakel, Ground state of electron gases at negative compressibility, Phys. Rev. B **64**, 245101 (2001).

[19] B. Skinner and B. I. Shklovskii, Anomalously large capacitance of a plane capacitor with a two-dimensional electron gas, Phys. Rev. B **82**, 155111 (2010).

[20] S. V. Kravchenko, D. A. Rinberg, S. G. Semenchinsky, and V. M. Pudalov, Evidence for the influence of electron-electron interaction on the chemical potential of the two-dimensional electron gas, Phys. Rev. B **42**, 3741 (1990).

[21] J. P. Eisenstein, L. N. Pfeiffer, and K. W. West, Negative Compressibility of Interacting Two-Dimensional Electron and Quasiparticle Gases, Phys. Rev. Lett. **68**, 674 (1992).

[22] J. P. Eisenstein, L. N. Pfeiffer, and K. W. West, Compressibility of the two-dimensional electron gas: Measurements of the zero-field exchange energy and fractional quantum Hall gap, Phys. Rev. B **50**, 1760 (1994).

[23] S. C. Dultz and H. W. Jiang, Thermodynamic Signature of a Two-Dimensional Metal-Insulator Transition, Phys. Rev. Lett. **84**, 4689 (2000).

[24] S. V. Kusminskiy, J. Nilsson, D. K. Campbell, and A. H. Castro Neto, Electronic Compressibility of a Graphene Bilayer, Phys. Rev. Lett. **100**, 106805 (2008).

[25] J. Junquera, P. García-Fernández, and M. Stengel, Mechanisms to enhance the capacitance beyond the classical limits in capacitors with free-electron-like electrodes, Phys. Rev. B **99**, 235127 (2019).

[26] W. Wen, G. Zhao, C. Hong, Z. Song, and R.-H. He, 3D negative electronic compressibility as a new emergent phenomenon, J. Supercond. Novel Magn. **33**, 229 (2020).

[27] L. Li, C. Richter, S. Paetel, T. Kopp, J. Mannhart, and R. Ashoori, Very large capacitance enhancement in a two-dimensional electron system, Science **332**, 825 (2011).

[28] V. Tinkl, M. Breitschaft, C. Richter, and J. Mannhart, Large negative electronic compressibility of $LaAlO_3$-$SrTiO_3$ interfaces with ultrathin $LaAlO_3$ layers, Phys. Rev. B **86**, 075116 (2012).

[29] A. E. M. Smink, J. C. de Boer, M. P. Stehno, A. Brinkman, W. G. van der Wiel, and H. Hilgenkamp, Gate-Tunable Band Structure of the $LaAlO_3$-$SrTiO_3$ Interface, Phys. Rev. Lett. **118**, 106401 (2017).

[30] A. Ohtomo and H. Hwang, Corrigendum: A high-mobility electron gas at the $LaAlO_3/SrTiO_3$ heterointerface, Nature **441**, 120 (2006).

[31] N. Reyren, S. Paetel, A. Caviglia, L. Kourkoutis, G. Hammerl, C. Richter, C. Schneider, T. Kopp, A.-S. Rüetschi, D. Jaccard, M. Gabay, D. Muller, J.-M. Triscone, and J. Mannhart, Superconducting interfaces between insulating oxides, Science **317**, 1196 (2007).

[32] J. Biscaras, N. Bergeal, S. Hurand, C. Grossetête, A. Rastogi, R. C. Budhani, D. LeBoeuf, C. Proust, and J. Lesueur, Two-Dimensional Superconducting Phase in $LaTiO_3/SrTiO_3$ Heterostructures Induced by High-Mobility Carrier Doping, Phys. Rev. Lett. **108**, 247004 (2012).

[33] A. Caviglia, S. Gariglio, N. Reyren, D. Jaccard, T. Schneider, M. Gabay, S. Paetel, G. Hammerl, J. Mannhart, and J.-M. Triscone, Electric field control of the $LaAlO_3/SrTiO_3$ interface ground state, Nature **456**, 624 (2009).

[34] C. Bell, S. Harashima, Y. Kozuka, M. Kim, B. G. Kim, Y. Hikita, and H. Y. Hwang, Dominant Mobility Modulation by the Electric Field Effect at the $LaAlO_3/SrTiO_3$ Interface, Phys. Rev. Lett. **103**, 226802 (2009).

[35] R. M. Fernandes, J. T. Haraldsen, P. Wölfle, and A. V. Balatsky, Two-band superconductivity in doped $SrTiO_3$ films and interfaces, Phys. Rev. B **87**, 014510 (2013).

[36] J. Haraldsen and A. Balatsky, Effects of magnetoelectric ordering due to interfacial symmetry breaking, Mater. Res. Lett. **1**, 39 (2013).

[37] G. Singh, A. Jouan, L. Benfatto, F. Couëdo, P. Kumar, A. Dogra, R. Budhani, S. Caprara, M. Grilli, E. Lesne *et al.*, Competition between electron pairing and phase coherence in superconducting interfaces, Nat. Commun. **9**, 407 (2018).

[38] H. Boschker, C. Richter, E. Fillis-Tsirakis, C. W. Schneider, and J. Mannhart, Electron-phonon coupling and the superconducting phase diagram of the $LaAlO_3$-$SrTiO_3$ interface, Sci. Rep. **5**, 12309 (2015).

[39] K. Dunnett, A. Narayan, N. A. Spaldin, and A. V. Balatsky, Strain and ferroelectric soft-mode induced superconductivity in strontium titanate, Phys. Rev. B **97**, 144506 (2018).

[40] C. Herrera, J. Cerbin, A. Jayakody, K. Dunnett, A. V. Balatsky, and I. Sochnikov, Strain-engineered interaction of quantum polar and superconducting phases, Phys. Rev. Materials **3**, 124801 (2019).

[41] C. S. Koonce, M. L. Cohen, J. F. Schooley, W. R. Hosler, and E. R. Pfeiffer, Superconducting transition temperatures of semiconducting $SrTiO_3$, Phys. Rev. **163**, 380 (1967).

[42] G. Binnig, A. Baratoff, H. E. Hoenig, and J. G. Bednorz, Two-Band Superconductivity in Nb-Doped $SrTiO_3$, Phys. Rev. Lett. **45**, 1352 (1980).

[43] V. Guduru, A. McCollam, J. Maan, U. Zeitler, S. Wenderich, M. Kruize, A. Brinkman, M. Huijben, G. Koster, D. Blank, G. Rijnders, and H. Hilgenkamp, Multi-band conduction behaviour at the interface of $LaAlO_3/SrTiO_3$ heterostructures, J. Korean Phys. Soc. **63**, 437 (2013).

[44] V. Guduru, A. Aguila, S. Wenderich, M. Kruize, A. McCollam, P. Christianen, U. Zeitler, A. Brinkman, G. Rijnders, H. Hilgenkamp, and J. Maan, Optically excited multi-band conduction in $LaAlO_3/SrTiO_3$ heterostructures, Appl. Phys. Lett. **102**, 051604 (2013).

[45] K. Song, S. Ryu, H. Lee, T. R. Paudel, C. T. Koch, B. Park, J. K. Lee, S.-Y. Choi, Y.-M. Kim, J. C. Kim *et al.*, Direct imaging of the electron liquid at oxide interfaces, Nat. Nanotechnol. **13**, 198 (2018).

[46] A. Joshua, S. Pecker, J. Ruhman, E. Altman, and S. Ilani, A universal critical density underlying the physics of electrons at the $LaAlO_3/SrTiO_3$ interface, Nat. Commun. **3**, 1129 (2012).

[47] J. L. M. van Mechelen, D. van der Marel, C. Grimaldi, A. B. Kuzmenko, N. P. Armitage, N. Reyren, H. Hagemann, and I. I. Mazin, Electron-Phonon Interaction and Charge Carrier Mass Enhancement in $SrTiO_3$, Phys. Rev. Lett. **100**, 226403 (2008).

[48] A. E. M. Smink, M. P. Stehno, J. C. de Boer, A. Brinkman, W. G. van der Wiel, and H. Hilgenkamp, Correlation between superconductivity, band filling, and electron confinement at the $LaAlO_3/SrTiO_3$ interface, Phys. Rev. B **97**, 245113 (2018).

[49] H. Suhl, B. T. Matthias, and L. R. Walker, Bardeen-Cooper-Schrieffer Theory of Superconductivity in the Case of Overlapping Bands, Phys. Rev. Lett. **3**, 552 (1959).

[50] R. Radebaugh and P. H. Keesom, Low-temperature thermodynamic properties of vanadium. I. Superconducting and normal states, Phys. Rev. **149**, 209 (1966).

[51] L. Y. L. Shen, N. M. Senozan, and N. E. Phillips, Evidence for Two Energy Gaps in High-Purity Superconducting Nb, Ta, and V, Phys. Rev. Lett. **14**, 1025 (1965).

[52] A. J. Bennett, Theory of the anisotropic energy gap in superconducting lead, Phys. Rev. **140**, A1902 (1965).

[53] J. D. Short and J. P. Wolfe, Evidence for Large Gap Anisotropy in Superconducting Pb from Phonon Imaging, Phys. Rev. Lett. **85**, 5198 (2000).

[54] P. G. Tomlinson and J. P. Carbotte, Anisotropic superconducting energy gap in Pb, Phys. Rev. B **13**, 4738 (1976).

[55] C. Bersier, A. Floris, P. Cudazzo, G. Profeta, A. Sanna, F. Bernardini, M. Monni, S. Pittalis, S. Sharma, H. Glawe, A. Continenza, S. Massidda, and E. K. U. Gross, Multiband superconductivity in Pb, H under pressure and CaBeSi from *ab-initio* calculations, J. Phys.: Condens. Matter **21**, 164209 (2009).

[56] D. C. Wallace, Thermodynamics of crystals, Am. J. Phys. **40**, 1718 (1972).

[57] P. P. Ruden and Z. Wu, Exchange effect in coupled two-dimensional electron gas systems, Appl. Phys. Lett. **59**, 2165 (1991).

[58] N. Scopigno, D. Bucheli, S. Caprara, J. Biscaras, N. Bergeal, J. Lesueur, and M. Grilli, Phase Separation from Electron Confinement at Oxide Interfaces, Phys. Rev. Lett. **116**, 026804 (2016).

[59] K. Steffen, R. Frésard, and T. Kopp, Capacitance and compressibility of heterostructures with strong electronic correlations, Phys. Rev. B **95**, 035143 (2017).

[60] S. Nagano, K. S. Singwi, and S. Ohnishi, Correlations in a two-dimensional quantum electron gas: The ladder approximation, Phys. Rev. B **29**, 1209 (1984).

[61] A. F. Santander-Syro, O. Copie, T. Kondo, F. Fortuna, S. Pailhès, R. Weht, X. G. Qiu, F. Bertran, A. Nicolaou, A. Taleb-Ibrahimi, P. Le Fèvre, G. Herranz, M. Bibes, N. Reyren, Y. Apertet, P. Lecoeur, A. Barthélémy, and M. J. Rozenberg, Two-dimensional electron gas with universal subbands at the surface of $SrTiO_3$, Nature **469**, 189 (2011).

[62] M. Huijben, A. Brinkman, G. Koster, G. Rijnders, H. Hilgenkamp, and D. H. Blank, Structure–property relation of $SrTiO_3/LaAlO_3$ interfaces, Adv. Mater. **21**, 1665 (2009).

[63] S. Gariglio, N. Reyren, A. D. Caviglia, and J.-M. Triscone, Superconductivity at the $LaAlO_3/SrTiO_3$ interface, J. Phys.: Condens. Matter **21**, 164213 (2009).

[64] D. van der Marel, J. L. M. van Mechelen, and I. I. Mazin, Common Fermi-liquid origin of T^2 resistivity and superconductivity in *n*-type $SrTiO_3$, Phys. Rev. B **84**, 205111 (2011).

[65] S. Gariglio, A. Fête, and J.-M. Triscone, Electron confinement at the $LaAlO_3/SrTiO_3$ interface, J. Phys.: Condens. Matter **27**, 283201 (2015).

[66] C. Bark, D. Felker, Y. Wang, Y. Zhang, H. Jang, C. Folkman, J. Park, S. Baek, H. Zhou, D. Fong *et al.*, Tailoring a two-dimensional electron gas at the $LaAlO_3/SrTiO_3$ (001) interface by epitaxial strain, Proc. Natl. Acad. Sci. U.S.A. **108**, 4720 (2011).

[67] R. C. Neville, B. Hoeneisen, and C. A. Mead, Permittivity of strontium titanate, J. Appl. Phys. **43**, 2124 (1972).

[68] R. Berg, P. Blom, J. Cillessen, and R. Wolf, Field dependent permittivity in metal-semiconducting $SrTiO_3$ Schottky diodes, Appl. Phys. Lett. **66**, 697 (1995).

[69] M. Sing, G. Berner, K. Goß, A. Müller, A. Ruff, A. Wetscherek, S. Thiel, J. Mannhart, S. A. Pauli, C. W. Schneider, P. R. Willmott, M. Gorgoi, F. Schäfers, and R. Claessen, Profiling the Interface Electron Gas of $LaAlO_3/SrTiO_3$ Heterostructures with Hard X-Ray Photoelectron Spectroscopy, Phys. Rev. Lett. **102**, 176805 (2009).

[70] A. Janotti, D. Steiauf, and C. G. Van de Walle, Strain effects on the electronic structure of $SrTiO_3$: Toward high electron mobilities, Phys. Rev. B **84**, 201304(R) (2011).

[71] H. Peelaers, K. Krishnaswamy, L. Gordon, D. Steiauf, A. Sarwe, A. Janotti, and C. Van de Walle, Impact of electric-field dependent dielectric constants on two-dimensional electron gases in complex oxides, Appl. Phys. Lett. **107**, 183505 (2015).

[72] O. Copie, V. Garcia, C. Bödefeld, C. Carrétéro, M. Bibes, G. Herranz, E. Jacquet, J.-L. Maurice, B. Vinter, S. Fusil, K. Bouzehouane, H. Jaffrès, and A. Barthélémy, Towards Two-Dimensional Metallic Behavior at $LaAlO_3/SrTiO_3$ Interfaces, Phys. Rev. Lett. **102**, 216804 (2009).

[73] I. V. Maznichenko, S. Ostanin, V. K. Dugaev, I. Mertig, and A. Ernst, Impact of long-range disorder on the two-dimensional electron gas formation at a $LaAlO_3/SrTiO_3$ interface, Phys. Rev. Materials **2**, 074003 (2018).

[74] H. Guo, W. A. Saidi, and J. Zhao, Tunability of the two-dimensional electron gas at $LaAlO_3/SrTiO_3$ interface by

strain-induced ferroelectricity, Phys. Chem. Chem. Phys. **18**, 28474 (2016).

[75] Z. Zhong, A. Tóth, and K. Held, Theory of spin-orbit coupling at $LaAlO_3/SrTiO_3$ interfaces and $SrTiO_3$ surfaces, Phys. Rev. B **87**, 161102(R) (2013).

[76] A. McCollam, S. Wenderich, M. Kruize, V. Guduru, H. Molegraaf, M. Huijben, G. Koster, D. H. Blank, G. Rijnders, A. Brinkman *et al.*, Quantum oscillations and subband properties of the two-dimensional electron gas at the $LaAlO_3/SrTiO_3$ interface, APL Mater. **2**, 022102 (2014).